Electronically excited and ionized states of the chlorine molecule

ARTICLE *in* CHEMICAL PHYSICS · MAY 1981

Impact Factor: 1.65 · DOI: 10.1016/0301-0104(81)80208-X

2 AUTHORS, INCLUDING:

Sigrid D Peyerimhoff
University of Bonn

488 PUBLICATIONS **15,998** CITATIONS

Chemical Physics 57 (1981) 279–296
North-Holland Publishing Company

ELECTRONICALLY EXCITED AND IONIZED STATES OF THE CHLORINE MOLECULE

Sigrid D. PEYERIMHOFF
Lehrstuhl für Theoretische Chemie, Universität Bonn, D-5300 Bonn 1, West Germany

and

Robert J. BUENKER
Lehrstuhl für Theoretische Chemie, Universität-Gesamthochschule Wuppertal, D-5600 Wuppertal 1, West Germany

Received 29 December 1980

Potential curves for the ground and excited states of the chlorine molecule and its positive and negative ions have been calculated by means of the MRD-CI method. The standard AO basis employed consists of 74 functions including two atomic d and one set of s and p bond species, and the results at the corresponding full CI level are estimated for each state via a perturbation correction. Special emphasis is placed upon the treatment of Rydberg–valence mixing in this system, which phenomenon is found to be essential to the understanding of the Cl_2 electronic absorption spectrum. All singlet states which correlate with the lowest dissociation limit plus many others which go to ionic $Cl^- + Cl^-$ or Rydberg Cl + Cl asymptotes are given explicit consideration. Among the triplet species of Cl_2 which dissociate into the ground state atoms only the $^3\Pi_u$ state is not repulsive. The calculated D_0 value for the ground state is 2.455 eV compared to the experimental value of 2.475 eV, while the vertical ionization energy and electron affinity are found to be 11.48 and 2.38 eV respectively, also in very good agreement with the corresponding measured data of 11.50 and 2.51 ± 0.1 eV. In addition the Cl_2 laser line is confirmed to result from a $^3\Pi_g \rightarrow {}^3\Pi_u$ emission, whereby the calculated downward vertical transition energy of 4.86 eV fits in quite well with the known location of this line at 4.805 eV. The first two dipole-allowed transitions from the ground state of chlorine involve $^1\Sigma_u^+$ and $^1\Pi_u$ states which are calculated to be nearly isoenergetic, and these results also match very well with the location of the first absorption band in this spectrum. Finally quite similarly as in O_2 it is found that an avoided crossing between Rydberg and valence states produces a relatively steep potential well for an upper state ($2\,^1\Sigma_u^+$), whose location coincides with that of a second absorption band recently observed in synchrotron radiation studies.

1. Introduction

The electronically excited states of chlorine have received increased attention over the past years, especially in connection with UV laser experiments [1–4]. Because of the relatively high stability of the upper laser levels against collisional deactivation by rare gas atoms such diatomic halogens (or interhalogens) are considered to be potential candidates for high-power lasers [4]. The laser emission in Cl_2 is observed at 258 nm [1], and it is assumed to result from a transition from an ionic upper state to a lower species of covalent character, whereby the identification of either state is as yet unsettled.

In an attempt to obtain more detailed spectroscopic information on the high-lying states of Cl_2 as well as on the dynamics of the excited species in halogen-doped rare gases synchrotron radiation has been employed for the Cl_2 excitation process [2, 3, 5] and the emission fluorescence has been studied for Cl_2 between 130 nm and 300 nm under various high- and low-pressure conditions. The most prominent excitation peak is observed at 135.4 nm [2] and the magnitude of its radiative life-time favors

assignment to a singlet state, the character of which is unknown. Further progressions are observed in absorption at higher frequencies [5] and various emission studies [5, 6] report broad structural features at lower energies which also await classification; the laser line itself appears with appreciable intensity at higher rare gas concentration, suggesting a triplet population as a result of a rare gas excimer–halogen interaction. The character of the initial state populated in the excitation is also not clear but based on qualitative arguments it is expected to be Rydberg in nature.

Under these circumstances it seems very advisable to undertake a systematic study of all Cl_2 states which dissociate to the first limits Cl + Cl and $Cl^+ + Cl^-$. Furthermore it must be assumed that mixing between Rydberg and valence states [7–11] plays a prominent part in the absorption and emission processes of Cl_2, just as in oxygen [7, 8, 11], for example, or in the photodecomposition of small hydrides such as NH_3 [12], and hence an investigation of the first members of the various Rydberg series also seems to be required in order to be able to analyze the data obtained under various experimental conditions.

The present work reports the results of such a study based on large-scale ab initio configuration interaction calculations, which have proven in the past to be a very powerful theoretical tool for the investigation of ground and excited surfaces of small polyatomic molecules, whereby an accuracy of 0.1–0.2 eV in excitation energies can generally be achieved [13] regardless of the multiplet structure or the special nature of the state. No spin–orbit effects are taken into account thereby but it is assumed that the essential features of the Cl_2 spectrum can be obtained for this study without having to account for such fine-structure aspects. All singlet states are treated explicitly in the present calculation whereas only a selection of various representative states is made from the triplet manifold. The results of this theoretical investigation should constitute a reliable basis for the interpretation of the measured data and should also serve as an excellent guide for further experimentation seeking to fully understand the spectroscopic and kinetic processes involving Cl_2 molecules.

2. Details of the theoretical treatment

The standard AO basis set employed in the present calculations consists of a total 74 contracted cartesian gaussian orbitals. The (12s8p) set given by Dunning and Hay [14] in the (5, 3, 1, 1, 1; 4, 2, 1, 1) contraction is augmented by two d functions with exponents 0.70 and 0.25 respectively and an additional (negative-ion) p function with exponent 0.049. For further improvement of the description of the charge distribution in the bonding region one s (exponent 1.0) and one p function (exponent 0.6) are added and are located directly in the middle of the Cl–Cl bond. In order to describe the first members of the Rydberg s and p series appropriate 4s (exponent 0.025) and 4p (exponent 0.020) gaussians are also located between the two chlorine nuclei.

For a few additional calculations this standard basis has been extended. First, in order to account for the first members of the Rydberg d series a set of diffuse d functions (exponent 0.017) is added at the center of the bond, but this has only been done at the equilibrium Cl_2 distance. Secondly, for proper dissociation to $Cl^* + Cl$ the single bond-centered 4s Rydberg function is replaced by two such species with the same exponent but centered at the respective nuclei; this calculation has only been carried out at 20 au, i.e. practically at the dissociation limit. This last replacement is entirely consistent with the other Rydberg-state calculations for the Cl_2 molecule since it has been shown [15] that for a molecular treatment one Rydberg s function located at the center of a bond (united atom) is entirely equivalent to the positive linear combination of two such species located at the two nuclear centers, whereby the negative linear combination in this case is equivalent to the Rydberg $p\sigma$ representation.

The configuration interaction calculations are of the multi-reference single- and double-excita-

tion (MRD-CI) type with configuration selection and energy extrapolation, as described in the literature [16, 17]. The energy corresponding to the full CI treatment has thereby been estimated via the relation

$$E_{\text{full CI}} = E_{\text{MRD-CI}} + (E_{\text{MRD-CI}} - E_{\text{ref}})\left[1 - \sum_{i}^{\text{ref}} c_i^2\right],$$

in analogy to the formula given by Davidson et al. [18] for the contribution of higher than double-excitation configurations relative to a single determinant. The technical details, i.e. number of reference configurations, number of roots according to which selection of configurations is undertaken, total number of generated configurations for which the energy is extrapolated as well as the average size of the secular equation which has actually been solved for the selected configurations, will be given together with the results in each instance. Generally only the ground state molecular orbitals are thereby employed throughout, and the treatment has been carried out for the sake of technical simplicity in the framework of the D_{2h} subgroup. Furthermore, a core of 10 molecular orbitals is assumed to remain doubly occupied for all geometries considered; these correspond to the 1s, 2s and $2p_x$, $2p_y$, $2p_z$ orbitals which are expected to show no contribution to the actual binding and to remain unchanged in the various states considered. Similar calculations for the excited states of H_2S, for example ref. [19], have supported this assumption numerically; even though the total energy is lowered by 2.5 eV upon releasing the restriction of a closed L shell, the excitation energies to four $^1B_1$ states are found to change by only from −0.01 eV to 0.03 eV upon allowing variable occupation of the 2s and 2p shells, variations well within the error limits of such standard treatments.

3. Singlet states corresponding to the first dissociation limit $Cl(^2P_u)+Cl(^2P_u)$

The combination $Cl(^2P_u)+Cl(^2P_u)$ results in a total of 9 singlet components, namely $2\times{}^1\Sigma_g^+$, $^1\Sigma_u^-$, $^1\Pi_u$ and $^1\Delta_g$, whose dominant electronic configurations are listed in table 1. The Cl_2 ground state possesses the electronic configuration $\sigma_g^2\pi_u^4\pi_g^4$, whereby at large internuclear distances because of the degeneracy of $\sigma_g(s+s)$ and $\sigma_u(s-s)$ the second configuration $\pi_u^4\pi_g^4\sigma_u^2$ gains equal weights (table 1). The calculated potential energy curve is plotted in fig. 1; the pertinent data obtained for this $X\,^1\Sigma_g^+$ state via a polynomial fit of the potential curve are listed in table 2 and it is seen that the theoretical representation of the experimental data is extremely good. The discrepancy in the equilibrium bond length is 0.03 Å, in the vibrational frequency less than 10 cm^{-1}, and in the dissociation energy only a few hundredths of an eV.

The other five states which correlate with the first Cl_2 dissociation limit all populate the strongly antibonding σ_u MO (table 1) and thus show repulsive behavior (at least below energies of −919.0000 hartree, in which range no mixing with Rydberg states can occur; see fig. 1). Double population of the σ_u orbital as in $^1\Sigma_u^-(\pi_u\pi_g\rightarrow\sigma_u^2)$ or $2\,^1\Sigma_g^+$ and $^1\Delta_g$ (both resulting from $\pi_g^2\rightarrow\sigma_u^2$ excitation; see table 1) thereby enhances the repulsive tendency so that $^1\Sigma_u^-$ is

Table 1
Dominant electronic configurations of the lowest 9 singlet states in Cl_2 excluding the Rydberg interaction at small internuclear distances

State	Excitation	Configuration	
		intermediate R	large R
$X\,^1\Sigma_g^+$		$\sigma_g^2\pi_u^4\pi_g^4\sigma_u^0$	$\sigma_g^0\pi_u^4\pi_g^4\sigma_u^2$ $\sigma_g^2\pi_u^4\pi_g^4\sigma_u^0$
$2\,^1\Sigma_g^+$	$\pi_g^2\rightarrow\sigma_u^2$ $(\pi_u^2\rightarrow\sigma_u^2)$	$\sigma_g^2\pi_u^4\pi_g^2\sigma_u^2$	$\sigma_g^2\pi_u^2\pi_g^4\sigma_u^2$ $\sigma_g^2\pi_u^4\pi_g^2\sigma_u^2$
$^1\Sigma_u^-$	$\pi_u\pi_g\rightarrow\sigma_u^2$	$\sigma_g^2\pi_u^3\pi_g^3\sigma_u^2$	$\sigma_g^2\pi_u^3\pi_g^3\sigma_u^2$
$^1\Pi_g$	$\pi_u\rightarrow\sigma_u$ $(\pi_g\sigma_g\rightarrow\sigma_u^2)$	$\sigma_g^2\pi_u^3\pi_g^4\sigma_u$	$\sigma_g^2\pi_u^3\pi_g^4\sigma_u$ $\sigma_g\pi_u^4\pi_g^3\sigma_u^2$
$^1\Pi_u$	$\pi_g\rightarrow\sigma_u$ $(\pi_u\sigma_g\rightarrow\sigma_u^2)$	$\sigma_g^2\pi_u^4\pi_g^3\sigma_u$	$\sigma_g^2\pi_u^4\pi_g^3\sigma_u$ $\sigma_g\pi_u^3\pi_g^4\sigma_u^2$
$^1\Delta_g$	$\pi_g^2\rightarrow\sigma_u^2$ $(\pi_u^2\rightarrow\sigma_u^2)$	$\sigma_g^2\pi_u^4\pi_g^2\sigma_u^2$	$\sigma_g^2\pi_u^4\pi_g^2\sigma_u^2$ $\sigma_g^2\pi_u^2\pi_g^4\sigma_u^2$

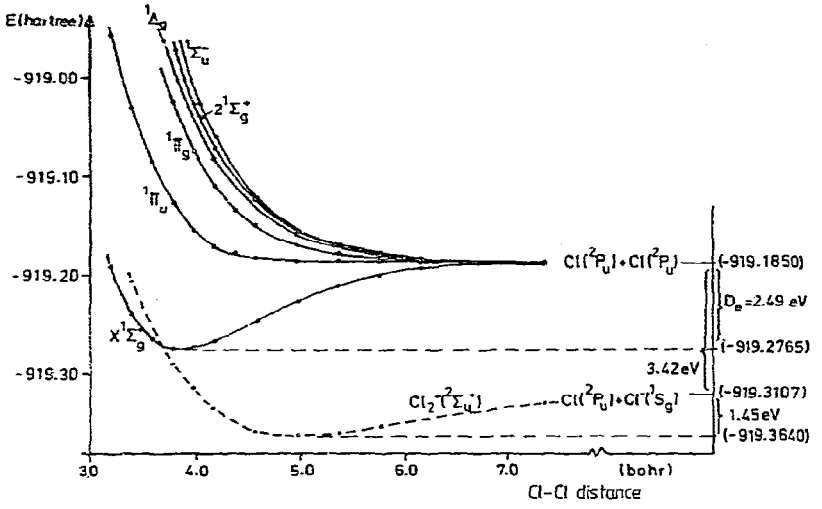

Fig. 1. Calculated potential energy curves for the chlorine states which dissociate into the lowest atomic limit. The corresponding ground state Cl_2^- curve is also given. In the present and all ensuing figures energy values are taken from the estimated full CI level of treatment.

calculated to be the most repulsive of all of these states while the $\pi_g \rightarrow \sigma_u$ replacement as in the $^1\Pi_u$ leads to an extremely flat potential energy curve (fig. 1); in the latter case the error limits of the calculations are such that a very weak potential minimum in this $^1\Pi_u$ state could also be possible.

The technical details of the calculations for these states are collected in table 3. For the ground and 2 $^1\Sigma_g^+$ states as well as for the $^1\Delta_g$ species various independent treatments have been undertaken in order to check the numerical consistency. The $^1\Delta_g$ symmetry can be obtained from either the ^1A_g or $^1B_{3g}$ represen-

Table 2
Calculated ground state data for Cl_2 (full CI estimate) and comparison with experimental results

	Theoretical	Experimental [a]
E_{SCF}	−918.91971	–
$E_{MRD\text{-}CI}$	−919.24332 [b]	–
$E_{full\,CI\,est.}$	−919.2760	–
$E_{\infty\,full\,CI\,est.}$	−919.185 [c]	–
r_0 (Å)	2.020	1.9879
ω_e (cm^{-1})	552	559.71
D_e (eV)	2.49	
D_0 (eV)	2.455 [d]	2.475±0.0003

[a] Ref. [20]. [b] At r=1.988 Å (in hartree).
[c] At r=20 bohr. [d] Calculated as $D_0=D_e-\omega_e/2$.

Table 3
Technical details for the calculations of the lowest singlet states in Cl_2. Given are the number of reference configurations (mains), number of roots according to which selection is carried out, the total number of symmetry adapted functions (SAFs) for which the energy extrapolation is undertaken, as well as the range of secular equations (depending on R) for which the diagonalization has actually been carried out

State	No. of mains	No. of roots	No. of total SAFs	No. of selected SAFs
$^1\Sigma_g^+$	15	4	197707	4600–5900
	8	2	95881	6400–7000
$^1\Sigma_u^-$	6	1	229816	3100–3600
$^1\Pi_g$	10	4	271896	4600–5900
$^1\Pi_u$	11	4	285691	4800–6900
$^1\Delta_g$	8	2	186651	2300–3200 [a]
	13	2	195994	2800–4800
	10	2	424770	4333 [b]

[a] In ^1A_g symmetry (D_{2h}). [b] In $^1B_{1g}$ symmetry (D_{2h}).

tation in the D_{2h} point group; the potential curve calculation has been undertaken in the computationally more appropriate (see table 3) ^1A_g representation. The numerical discrepancy between the $^1B_{3g}$ and ^1A_g energy at a distance of 4.157 bohr (2.2 Å) was thereby 0.003 hartree for the first and −0.002 hartree for the second valence $^1\Delta_g$ state. It should also be pointed out that even though $^1\Sigma_g^+$ and $^1\Delta_g$ state result from the same representation in D_{2h}, the selection is undertaken for only one $D_{\infty h}$ symmetry type in a given calculation, so that the 4-root selection for the $^1\Sigma_g^+$ states in table 3 considers no $^1\Delta_g$ species.

4. Positive and negative ionic states

Since the Rydberg states play an essential role for excitation processes from the ground state and for the deactivation mechanisms arising because of the mixing of Rydberg and valence states, it seems appropriate to first study the various low-lying positive ion states since they constitute the envelope for the Rydberg manifold. The calculated potential energy curves for the $^2\Pi_g$, $^2\Pi_u$ and $^2\Sigma_g^+$ states are thus plotted in fig. 2, while the technical details for all these calculations are summarized in table 4.

As expected the lowest state results from ionization out of the π_g MO (see table 5), leading to a potential curve with a slightly smaller optimal equilibrium distance (table 6) than the Cl_2 ground state. By the same qualitative reasoning the ionization out of the bonding π_u results in a larger equilibrium bond length relative to the Cl_2 ground state; the situation is more complicated for the $^2\Sigma_g^+$ ion since two competitive processes (configurations $\sigma_g\pi_u^4\pi_g^4$ and $\sigma_g^2\pi_u^3\pi_g^3\sigma_u$, see table 5) are reponsible for the avoided crossing in the $^2\Sigma_g^+$ potential surfaces.

The calculated vertical excitation energy of 11.48 eV to the Cl_2^+ $^2\Pi_g$ state is in excellent agreement with the average peak derived from photoelectron spectra (11.50 eV, table 6). The higher ionization peaks are not known very accurately, but the estimated values of approximately 20000 cm^{-1} ($^2\Pi_u$) and 34400 cm^{-1} ($^2\Sigma_g^+$) match (within the uncertainties) quite well the calculated data. The atomic ionization limit calculated at −918.725 hartree (in a Cl_2^+ calculation at 20 bohr) is too low by 0.4–0.5 eV, but such an underestimation for higher

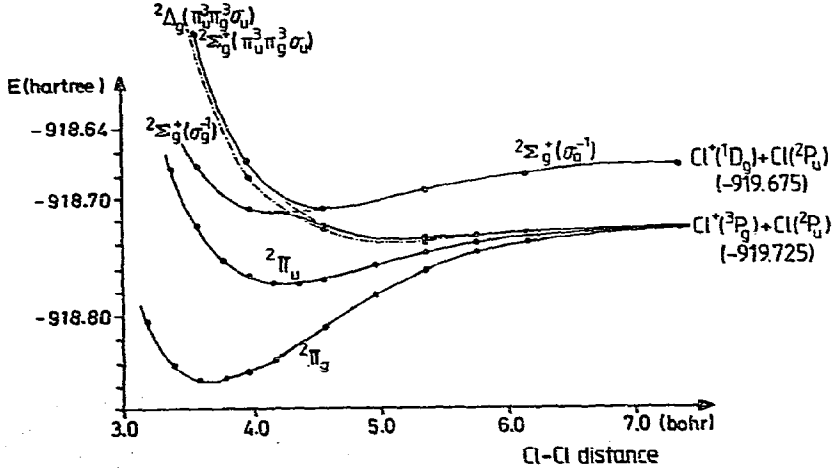

Fig. 2. Calculated potential energy curves for the lowest electronic states of Cl_2^+. Note that not all of the states correlating with the atomic limits shown are calculated.

Table 4
Technical details for the calculations of the first three positive Cl_2^+ ions and for the first negative ion state. The nomenclature is the same as employed in table 3

State	No. of mains	No. of roots	No. of total SAFs	No. of selected SAFs
$^2\Pi_g$	7	1	231136	2800–3500
$^2\Pi_u$	8	1	288771	2900–3500
$^2\Sigma_g^+$	5	3	140897	4800–6000
	9	3	304004	4500–5500
negative ion				
$^2\Sigma_u^+$	9	2	375368	5200–6500

dissociation limits have been noted before in similar calculations on N_2, for example [24], and it is known that a more proper description of the higher dissociation limits generally requires an even more extended AO basis set. Hence in the present case the ionic curves are expected to be somewhat too shallow, a fact which is reflected in the slightly larger r_e value and the smaller vibrational frequency in the calculations as seen for the $^2\Pi_g$ state in table 6; this behavior is also expected to hold for the other ionic states for which the experimental results are quite uncertain.

The Cl_2^- negative ion potential curve is also calculated and plotted in fig. 1. A minimum is found to occur around 2.66 Å (5.03 bohr) at an energy of −919.364 hartree. The calculated electron affinity (ΔE_e between Cl_2 and Cl_2^-) is thus 2.38 eV, in good accord with the experimental value of 2.51 eV ± 0.1 eV given in the literature [25]. The calculated dissociation energy is $D_e = 1.45$ eV, i.e. a somewhat larger value than the 1.26 eV derived in a combination of previous theoretical and experimental data [26]. The energy difference between the Cl_2 and Cl_2^- curves at very large internuclear distances is 3.42 eV [$E_\infty(Cl_2^-) = -919.3107$ hartree], which value should be compared with the known electron affinity of Cl of 3.61 eV. In summary then the positive and negative ion curves reproduce the measured Cl_2 data in a very good manner wherever comparison with experimental inferences is possible, and they yield new information which should be of analogous accuracy.

Table 5
Dominant electronic configurations of the low-lying positive and negative states of Cl_2

State	Ionization [a]	Configuration	
		intermediate R	larger R
$^2\Pi_g$	$\pi_g \rightarrow \infty$	$\sigma_g^2\pi_u^4\pi_g^3$	$\sigma_g^2\pi_u^4\pi_g^3$ $\pi_u^3\pi_g^3\sigma_u^2$
$^2\Pi_u$	$\pi_u \rightarrow \infty$	$\sigma_g^2\pi_u^3\pi_g^4$	$\sigma_g^2\pi_u^3\pi_g^4$ $\pi_u^3\pi_g^4\sigma_u^2$
$^2\Sigma_g^+$	$\sigma_g \rightarrow \infty$	$\sigma_g\pi_u^4\pi_g^4$	$\sigma_g^2\pi_u^3\pi_g^3\sigma_u$
$^2\Sigma_g^-$	$\pi_u\pi_g \rightarrow \sigma_u, \infty$	$\sigma_g^2\pi_u^3\pi_g^3\sigma_u$	$\sigma_g\pi_u^4\pi_g^2\sigma_u^2$
$^2\Sigma_u^+$ (negative ion)	σ_u	$\sigma_g^2\pi_u^4\pi_g^4\sigma_u$	$\sigma_g^2\pi_u^4\pi_g^3\sigma_u$

[a] Relative to the Cl_2 ground state configuration.

5. Singlet 4s and 4p Rydberg states and their interaction with the valence-shell species

The lowest Rydberg states result from π_g excitation and converge to the lowest positive ion state $^2\Pi_g$. The first members thereby are

$\pi_g \rightarrow 4s$, $^1\Pi_g$,

$\pi_g \rightarrow 4p\sigma$, $^1\Pi_u$,

$\pi_g \rightarrow 4p\pi$, $^1\Sigma_u^-$, $^1\Delta_u$, $^1\Sigma_u^+$.

Similarly, the first members converging to the *second* ionization potential $^2\Pi_u$ result from excitation of the π_u MO in an analogous manner, namely

$\pi_u \rightarrow 4s$, $^1\Pi_u$,

$\pi_u \rightarrow 4p\sigma$, $^1\Pi_g$,

$\pi_u \rightarrow 4p\pi$, $^1\Sigma_g^-$, $^1\Delta_g$, $^1\Sigma_g^+$.

They are expected to lie above the respective π_g counterparts by approximately the same amount as the $^2\Pi_u$ lies above the $^2\Pi_g$ ion. Furthermore, because of the non-bonding properties of the upper Rydberg orbitals the unperturbed poten-

Table 6
Calculated data for the Cl_2 positive ions and comparison with exeriment whenever possible

	$^2\Pi_g$		$^2\Pi_u$		$^2\Sigma_g^+$	
	calc.	exptl. [a]	calc.	exptl.	calc.	exptl.
ΔE_e (vertical)	11.48	IP = 11.50 (average of PES)	14.23		16.02	
T_e (eV)	11.44		13.73	(13.98) [b]	15.4 [d]	(15.76) [c]
r_e (Å)	1.92	1.89	2.27	(2.32) (2.28) (2.30)		
ω_e (cm^{-1})	620	644	380			
E_∞ (hartree)	−918.725	–				
$\Delta E(Cl^+, Cl)$ (eV)	12.52	12.96 (13.01)				

[a] From refs. [20, 22, 23]. [b] Approximately 20000 cm^{-1} above $^2\Pi_g$. [c] Approximately 34400 cm^{-1} above $^2\Pi_g$.
[d] σ_g^{-1} configuration.

tial curves for the Rydberg states are expected to run roughly parallel to the corresponding ionic curves discussed in the previous section.

Since there are a number of valence states in the same energy range as the Rydberg states, heavy perturbation or mixing of states is expected, however. First of all, at very small internuclear distances an interaction with the repulsive part of the states (fig. 1) dissociating to the ground state products $Cl(^2P_u)+Cl(^2P_u)$ is possible. Secondly, states which dissociate to the second dissociation limit $Cl^-(^1S_g)+Cl^+(^1D_g)$ accessible for singlet species are expected to mix with the Rydberg manifold at intermediate and larger Cl–Cl bond lengths; their configuration characteristics are summarized in table 7.

5.1. $^1\Pi_g$ states

A typical pattern for the interaction of states is contained in fig. 3 for the various $^1\Pi_g$ states. It is seen that the unperturbed Rydberg states resulting from $\pi_g \rightarrow 4s$ and $\pi_u \rightarrow 4p\sigma$ excitations closely parallel the potential surfaces of the respective positive ions, as expected. At very small internuclear distances the repulsive $1\,^1\Pi_g$ ($\pi_u \rightarrow \sigma_u$) interacts with the $\pi_g \rightarrow 4s$ Rydberg state while the second $^1\Pi_g$ state of valence characteristics dissociating to $Cl^-(^1S_g)+Cl^+(^1D_g)$ interacts with both $\pi_g \rightarrow 4s$ and $\pi_u \rightarrow 4p\sigma$ Rydberg species. As a consequence the potential energy surfaces resulting from the various avoided crossings are rather complex with a number of maxima and minima.

It should also be noted that while the $\pi_g \rightarrow 4s$ and $\pi_u \rightarrow 4p\sigma$ potential curves are practically

Table 7
Dominant electronic configurations of the Cl_2 singlet state which correlate with the dissociation limit $Cl^-(^1S_g)+Cl(^1D_g)$

State	Excitation	Configuration	
		intermediate R	large R
$^1\Sigma_g^+$	$\sigma_g^2 \rightarrow \sigma_u^2$	$\sigma_g^0\pi_u^4\pi_g^4\sigma_u^2$	$\sigma_g^2\pi_u^4\pi_g^4$ $\sigma_g^0\pi_u^4\pi_g^4\sigma_u^2$
$^1\Sigma_u^+$	$\sigma_g \rightarrow \sigma_u$	$\sigma_g\pi_u^4\pi_g^4\sigma_u$	$\sigma_g\pi_u^4\pi_g^4\sigma_u$
$^1\Pi_g$	$\sigma_g\pi_g \rightarrow \sigma_u^2$ $(\pi_u \rightarrow \sigma_u)$	$\sigma_g\pi_u^4\pi_g^3\sigma_u^2$	$\sigma_g\pi_u^4\pi_g^3\sigma_u^2$ $\sigma_g^2\pi_u^3\pi_g^4\sigma_u$
$^1\Pi_u$	$\pi_u\sigma_g \rightarrow \sigma_u^2$ $(\pi_g \rightarrow \sigma_u)$	$\sigma_g\pi_u^3\pi_g^4\sigma_u^2$	$\sigma_g\pi_u^3\pi_g^4\sigma_u^2$ $\sigma_g^2\pi_u^4\pi_g^3\sigma_u$
$^1\Delta_g$	$\pi_u^2 \rightarrow \sigma_u^2$ $(\pi_g^2 \rightarrow \sigma_u^2)$	$\pi_u^2\pi_g^4\sigma_u^2$	$\sigma_g^2\pi_u^2\pi_g^4\sigma_u^2$ $\sigma_g^2\pi_u^4\pi_g^2\sigma_u^2$
$^1\Delta_u$	$\pi_u\pi_g \rightarrow \sigma_u^2$	$\sigma_g^2\pi_u^3\pi_g^3\sigma_u^2$	$\sigma_g^2\pi_u^3\pi_g^3\sigma_u^2$

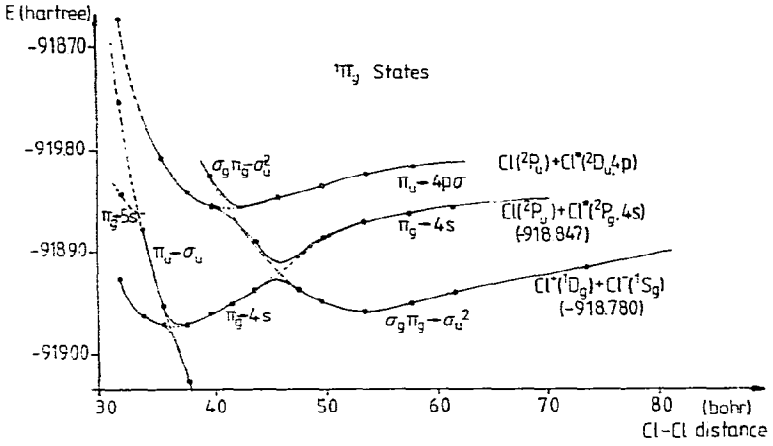

Fig. 3. Calculated potential energy curves for the lowest-lying $^1\Pi_g$ states of Cl_2, illustrating the mixing of Rydberg and valence states in this molecule. In the crossing regions estimates for the corresponding diabatic potential curves are shown as dashed lines in this and all ensuing figures.

horizontal at large internuclear distances, connecting to the neutral Cl^* (^2P_u, 4s) + Cl (^2P_u) and Cl^* (^2D_u, 4p) + Cl (^2P_u) products, the valence $^1\Pi_g$ curve shows an asymptotic $1/r$ behavior for large bond lengths, as to be expected from the electrostatic attraction of two charges, in this case Cl^- (^1S_g) and Cl^+ (^1D_g). The same pattern is present for all other states which dissociate into Cl^- and Cl^+ atoms. It should also be noted that the Cl^- (^1S_g) + Cl^+ (^1D_g) and Cl^* (^2P_g, 4s) + Cl (^2P_u) limits lie fairly close in energy according to the experimental data [$Cl^- = -3.61$ eV, Cl^+ (^1D_g) = 12.96 + 1.44 eV, $Cl^*(^2P_g, 4s) = 9.24$ eV], the pertinent ionic products thereby lie higher in energy by 1.55 eV. The present calculations yield the limiting value $E_\infty(\pi_g \rightarrow 4s) = -918.847$ hartree, while extrapolation for the ionic valence state according to $1/r$ gives −918.780 hartree. Comparison with the calculated value $E_\infty[Cl(^2P_u) + Cl(^2P_u)]$ in table 2 of −919.185 hartree yields calculated dissociation limits of 11.02 eV (10.79 eV, exptl.) for the singlet ions, and 9.20 eV (9.24 eV, exptl.) for the bond breakage leading to the excited neutral species. These calculations are carried out simultaneously for all four roots as indicated in table 3.

5.2. $^1\Pi_u$ states

All four $^1\Pi_u$ states are also obtained from the same secular equation (table 3). The analogous shape of the potential energy curve for the $\pi_g \rightarrow 4p\sigma$ and $\pi_u \rightarrow 4s$ states as that of the corresponding $^2\Pi_g$ and $^2\Pi_u$ ions is again obvious from fig. 4. Since the repulsive $1\,^1\Pi_u$ is the lowest energy curve of the states dissociating to the two Cl atoms in their ground state (fig. 1) it shows very little interaction with the first $^1\Pi_u$ Rydberg state in the interesting area of the potential minimum, in contrast to the previously discussed behavior of $1\,^1\Pi_g$; an analogous interaction will occur in the repulsive part of the $^1\Pi_u(\pi_g \rightarrow 4p\sigma)$ Rydberg state but this point has not been pursued in detail. Just as for the $^1\Pi_g$ manifold of states the ionic $^1\Pi_u$ species with $\pi_u\sigma_g \rightarrow \sigma_u^2$ excitation cuts through both the $\pi_g \rightarrow 4p\sigma$ and $\pi_u \rightarrow 4s$ Rydberg state potential curves leading to the various avoided crossings indicated in fig. 4. The calculated dissociation limits are −918.780 hartree for the $Cl^+(^1D_g)$ + $Cl^-(^1S_g)$ products and −918.846 hartree for the separation into $Cl^*(^2P_g, 4s) + Cl(^2P_u)$, i.e. 0.001 hartree different from the calculations in the $^1\Pi_g$ configurational space. Finally, the $\pi_g \rightarrow 5p\sigma$ potential energy curve is also obtained in the

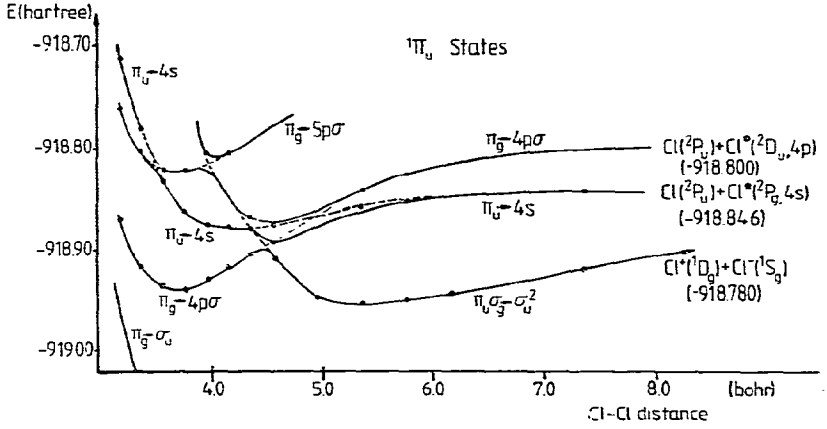

Fig. 4. Calculated potential energy curves for the lowest-lying $^1\Pi_u$ states of Cl_2, illustrating the mixing of Rydberg and valence states.

present AO basis, but its location might be somewhat too high since no explicit $5p\sigma$ functions have been included in the AO basis set; not unexpectedly it shows a parallel behavior to the lower $\pi_g \rightarrow 4p\sigma$ curve.

5.3. $^1\Sigma_u^+$ states

A detailed study of the $^1\Sigma_u^+$ states has been undertaken since $1\,^1\Sigma_u^+$ is the lowest state of the group given in table 7 which dissociates into the ionic species $Cl^+ + Cl^-$. It is also allowed to combine directly with the ground state and because of its Σ symmetry presumably does so with higher intensity than the (allowed) $^1\Pi_u$ just treated. Calculations are carried out for at least three different levels of accuracy at all internuclear distances (as indicated in table 8) in order to obtain as well as possible the estimate for the full CI energies [27] of the three lowest $^1\Sigma_u^+$ states.

The corresponding results are plotted in fig. 5. The potential curve of the $\pi_g \rightarrow 4p\pi$ Rydberg state, again in principle parallel to that for $^2\Pi_g$, is perturbed twice: by the lower energy $\sigma_g \rightarrow \sigma_u$ valence state close to its minimum, and by the second valence state of this symmetry possessing the $\sigma_g^2\pi_u^3\pi_g^3\sigma_u^2$ electronic configuration. As a result of these various avoided crossings the lowest-energy $^1\Sigma_u^+$ state possesses a quite shallow minimum at small internuclear distances, from which the deeper and more pronounced well around 5 bohr can probably be easily accessed by tunnelling or vibrational excitation. At the same time a further quite deep potential minimum is established for the $2\,^1\Sigma_u^+$ as a result of the avoided crossings of the $\sigma_g \rightarrow \sigma_u$ valence state (left branch) and $\pi_g \rightarrow 4p\pi$ Rydberg species. This latter state is only bound up to approximately -918.880 hartree, at which point it reaches a maximum with the vibrational levels connecting with those of the shallow potential curve running roughly parallel to the $1\,^1\Sigma_u^+$ at larger internuclear distances.

Table 8
Technical details for the calculations of the various states of $^1\Sigma_u^+$ symmetry

State	No. of mains	No. of roots	No. of total SAFs	No. of selected SAFs
$^1\Sigma_u^+$	14	3	323214	9200–9800
	9	3	182019	9100–9900
	5	3	105469	7000–9900
	11	2	283659	5400–6900
	13	2	305835	5700–6000
	8	2	159460	5900–6900

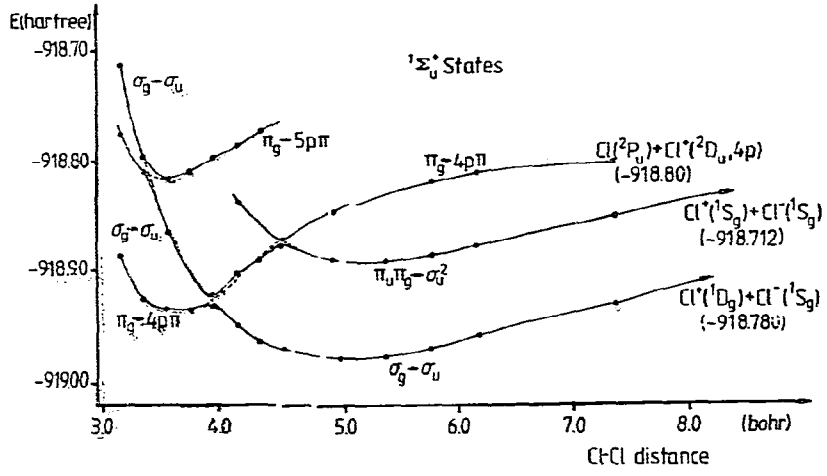

Fig. 5. Calculated potential energy curves for the lowest-lying $^1\Sigma_u^+$ states of Cl_2, illustrating the mixing of Rydberg and valence states.

This situation is very similar to that found for the $B^3\Sigma_u^-$ state in O_2 and its Rydberg states of the same symmetry [8, 10, 11]. In this molecule the first valence state is more repulsive and hence crosses the Rydberg species in such a manner that practically no minimum but only a shoulder remains at small internuclear distances; the quite shallow well at large bond lengths is responsible for the discrete Schumann–Runge bands resulting from transitions out of $X^3\Sigma_g^-$ ($v''=0$) to various vibrational levels in the $B^3\Sigma_u^-$ state, which correlates with the second dissociation $O(^3P_g)+O(^1D_g)$. The second $^3\Sigma_u^-$ well in O_2 is also quite deep; combination of $v'=0, 1, 2$ vibrational levels with $v''=0$ of the oxygen ground state give rise to the well-known relatively strong "first", "second" and "third" bands to the high-energy side of the Schumann–Runge continuum. In the present case the $2\,^1\Sigma_u^+$ surface is a very close analogue to the above and should also give rise to strong absorption bands with a vibrational frequency larger than in any other Rydberg or purely valence states of Cl_2; the corresponding intensity distribution should not be solely governed by the Franck–Condon principle since the electronic transition moment, just as in the parallel situation of O_2, changes dramatically over the vibrational amplitudes because of the change from a valence to a Rydberg-like species. Indeed, a vibrational pattern has been observed in this energy range [28] which can easily be assigned to $2\,^1\Sigma_u^+-X\,^1\Sigma_g^+$ chlorine transitions.

Higher-energy states, such as $\pi_g\rightarrow 5p\pi$, should possess potential curves running essentially parallel to that of the lowest-energy Rydberg species and the probability for an avoided crossing will be enhanced due to the greater density of states in this higher-energy region. It should again be pointed out that no $\pi_g\rightarrow 4d$ states have been treated, which are also expected to play a role at higher energies (see table 11).

5.4. $^1\Sigma_u^-$, $^1\Delta_u$, $^1\Delta_g$, $^1\Sigma_g^+$ and $^1\Sigma_g^-$ states

Since there is no $^1\Sigma_u^-$ state dissociating into Cl^-+Cl^+, the potential curve pattern is simpler than in the previous cases. The Rydberg state $\pi_g\rightarrow 4p\pi$ is intersected as expected by the repulsive $1\,^1\Sigma_u^-$ already discussed in fig. 1, but very little mixing is observed in this case (fig. 6). Hence both states could be treated for the most part in separate calculations, whereby the reference set for the Rydberg calculation consists of six configurations. The latter curve is

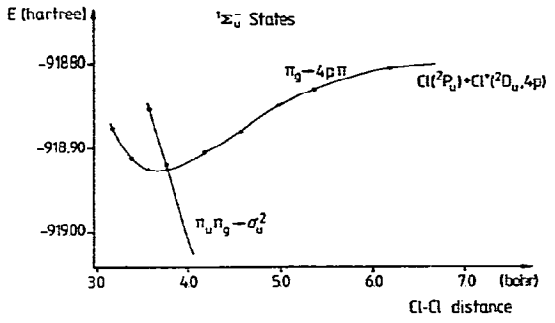

Fig. 6. Calculated potential energy curves for the lowest-lying $^1\Sigma_u^+$ states of Cl_2. The crossing between the two states is sharply avoided.

very close to the unperturbed $^1\Sigma_u^+(\pi_g \rightarrow 4p\pi)$ and $^1\Pi_u(\pi_g \rightarrow 4p\sigma)$ potential surfaces, as is expected because the various Rydberg members of the spatially different but otherwise energetically degenerate orbitals generally lie within a few tenths of an eV of one another. There is no second Rydberg state resulting from π_u excitation, contrary to the previous cases, and higher states of this symmetry have not been studied in the present work.

The results for the $^1\Delta_u$ and $^1\Delta_g$ states in the energy range considered are seen in fig. 7. Only one low-lying Rydberg state exists, namely $^1\Delta_u$ resulting from $\pi_g \rightarrow 4p\pi$ excitation. The corresponding $^1\Delta_g$ state is the $4p\pi$ member of the π_u-Rydberg series and has not been calculated. Its location and potential curve shape should be very close to that of the $\pi_u \rightarrow 4p\sigma(^1\Pi_g)$ state discussed earlier. Since there is no $^1\Delta_u$ repulsive state correlating with the ground state dissociation limit the $^1\Delta_u$ Rydberg surface remains unperturbed around its minimum. On the other hand the $^1\Delta_u(\sigma_g^2\pi_u^3\pi_g^3\sigma_u^2)$ state (table 7) which dissociates to the $Cl^+ + Cl^-$ limit mixes with the Rydberg curve in a similar manner as has been observed in the previous cases. The calculations have been technically carried out separately for Rydberg and valence states for most distances, whereby six reference configurations are taken for each of the valence and Rydberg species, while a 12 main/2 root calculation is undertaken in the mixing area. The $^1\Delta_g$ state has been obtained from the same secular equation as the first state of this symmetry (table 3) but could generally be of somewhat lower accuracy since the sum of the squares of the coefficients of the reference configurations $\sum_i^{ref} c_i^2$ is only around 0.87 compared to a value of 0.91 for the first such state.

The lowest $^1\Sigma_g^-$ state is of Rydberg nature and results from $\pi_u \rightarrow 4p\pi$ excitation. It has not been calculated since the lower energy part will probably not be perturbed because there are no states of this symmetry which correlate with

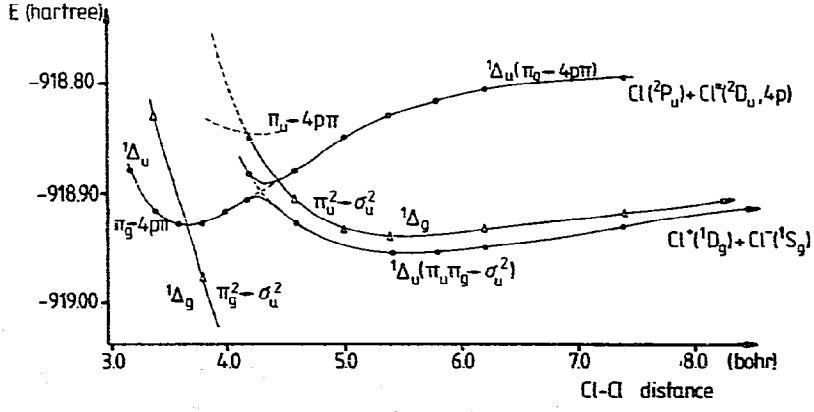

Fig. 7. Calculated potential energy curves for the lowest-lying $^1\Delta_g$ and $^1\Delta_u$ states of Cl_2. The location of the $\pi_u \rightarrow 4p\pi$ Rydberg potential curve is only estimated in the figure.

either the $Cl(^2P_u)+Cl(^2P_u)$ or the $Cl^-(^1S_g)+Cl^+(^1D_g)$ limit. The first Rydberg state of $^1\Sigma_g^+$ symmetry results from the same electronic excitation, $\pi_u \rightarrow 4p\pi$ or alternatively from $\sigma_g \rightarrow 4s$ transitions. Since both are relatively high in energy these states have also not been determined explicitly. The two high-lying valence states dissociating into $Cl^+(^1D_g)+Cl^-(^1S_g)$ and $Cl^+(^1S_g)+Cl^-(^1S_g)$ have been treated on the other hand, and show quite parallel behavior (fig. 8). Their calculated limits are −918.782 hartree and −918.712 hartree, in quite good accord with the limits calculated for the other states (−918.780 hartree, for $^1\Pi_g$ and $^1\Pi_u$) and also in good agreement with the corresponding experimental excitation energies, i.e. 10.96 eV (10.79 eV experimental) and 12.87 eV (experimental value approximately 3.45 eV higher than ^3P_g, i.e. 12.80 eV) above $Cl(^2P_u)+Cl(^2P_u)$.

6. Triplet states

The potential energy curves for the triplet states of Cl_2 show the same general pattern as has been discussed for the singlet manifold. There is first the group of repulsive (or almost repulsive) states which correlate with the ground state dissociation limit and show interaction with Rydberg species only in their strongly repulsive branch at very small internuclear distances. Secondly there is the family of states which converges to the ionic limit $Cl^-(^3P_g)+Cl^-(^1S_g)$, which energetically coincides essentially with the $Cl(^2P_u)+Cl^*(^2P_g, 4s)$ dissociation, whereby the potential curves for the ionic states can be represented for large internuclear distances simply by the $1/r$ attractive term but show essential mixing with Rydberg states at smaller internuclear separation. And finally there are the various Rydberg triplet states at practically the same energetic location as the corresponding singlet species because of the small singlet–triplet splitting (within a few tenths of an eV) in Rydberg states in general, whereby their potential curves run to a large extent parallel to the curves of the respective ionic species to which they converge. Transitions from small-distance minima to potential wells at large separations will thus involve motion through barriers connecting Rydberg and predominantly ionic states.

Of the six triplet states $^3\Sigma_u^+(2)$, $^3\Sigma_g^-$, $^3\Pi_g$, $^3\Pi_u$ and $^3\Delta_g$ which dissociate into the ground state products, only the $^3\Sigma_u^+$, $^3\Pi_g$ and $^3\Pi_u$ states have been treated in the present study. Similarly only the lowest states $^3\Pi_g$ and $^3\Pi_u$ which correlate with the ionic dissociation limit are calculated, while the others, namely $^3\Sigma_g^-$ and $^3\Sigma_u^-$, are omitted from explicit consideration. The various technical details along with the characterization of the different states are contained in tables 9 and 10.

The lowest $^3\Pi_u$ state is the only excited Cl_2 triplet state which has been studied in detail experimentally [29, 30] to the best of our

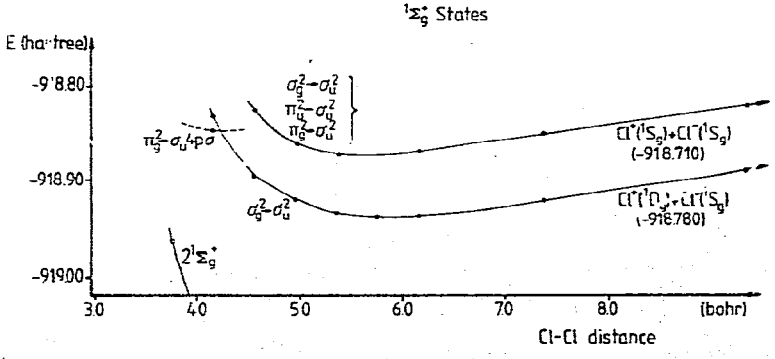

Calculated potential energy curves for the $^1\Sigma_g^+$ states correlating with the two lowest ionic limits.

Table 9
Dominant electronic configurations of the Cl_2 triplet states treated in the present work

State	Excitation	Configuration	
		intermediate R	large R
$^3\Pi_u$	$\pi_g \rightarrow \sigma_u$ ($\sigma_g\pi_u \rightarrow \sigma_u^2$)	$\pi_g^2\pi_u^4\pi_g^3\sigma_u$	$\sigma_g^2\pi_u^4\pi_g^3\sigma_u$ $\sigma_g\pi_u^3\pi_g^4\sigma_u^2$
$^3\Pi_g$	$\pi_u \rightarrow \sigma_u$ ($\sigma_g\pi_g \rightarrow \sigma_u^2$)	$\sigma_g^2\pi_u^3\pi_g^4\sigma_u$	$\sigma_g^2\pi_u^3\pi_g^4\sigma_u$ $\sigma_g\pi_u^4\pi_g^3\sigma_u^2$
$1^3\Sigma_u^+$	$\sigma_g \rightarrow \sigma_u$	$\sigma_g\pi_u^4\pi_g^4\sigma_u$	$\sigma_g\pi_u^4\pi_g^4\sigma_u$
$2^3\Sigma_u^+$	$\pi_u\pi_g \rightarrow \sigma_u^2$	$\sigma_g^2\pi_u^3\pi_g^3\sigma_u^2$	$\sigma_g^2\pi_u^3\pi_g^3\sigma_u^2$
$2^3\Pi_u$	$\sigma_g\pi_u \rightarrow \sigma_u^2$ ($\pi_g \rightarrow \sigma_u$)	$\sigma_g\pi_u^3\pi_g^4\sigma_u^2$	$\sigma_g\pi_u^3\pi_g^4\sigma_u^2$ $\sigma_g^2\pi_u^4\pi_g^3\sigma_u$
$2^3\Pi_g$	$\pi_g\sigma_g \rightarrow \sigma_u^2$ ($\pi_u \rightarrow \sigma_u$)	$\sigma_g\pi_u^4\pi_g^3\sigma_u^2$	$\sigma_g\pi_u^4\pi_g^3\sigma_u^2$ $\sigma_g^2\pi_u^3\pi_g^4\sigma_u^2$

knowledge. It shows a shallow minimum (fig. 9) which the calculations locate around 2.43 Å, i.e. at somewhat larger bond lengths than the experimental studies (2.396 Å). Considering the shallow form of the potential and furthermore the fact that data points have only been generated at 2.31 Å, 2.41 Å and 2.61 Å around the minimum such a discrepancy is not surprising. The two lowest $^3\Sigma_u^+$ states as well as the $^3\Pi_g$ species are all repulsive (fig. 9), just as has been found for all the singlet states which correlate with the ground state products (fig. 1); again double population of the σ_u MO as in the two $^3\Sigma_u^+$ states thereby enhances the repulsive character.

Table 10
Technical details for the calculations of the various triplet states treated in the present work

State	No. of mains	No. of roots	No. of total SAFs	No. of selected SAFs
$^3\Pi_u$	11	4	508631	5400–8100
$^3\Pi_g$	10	4	485807	4000–6000
$^3\Sigma_u^+(\sigma_g\sigma_u)$	4	1	123496	3300–3800
$^3\Sigma_u^+(\pi_u^3\pi_g^3)$	7	1	454021	3000–3300
$^3\Sigma_u^+$	9	2	506837	6000–6200
$^3\Sigma_u^+$	10	3	441538	4700–5100

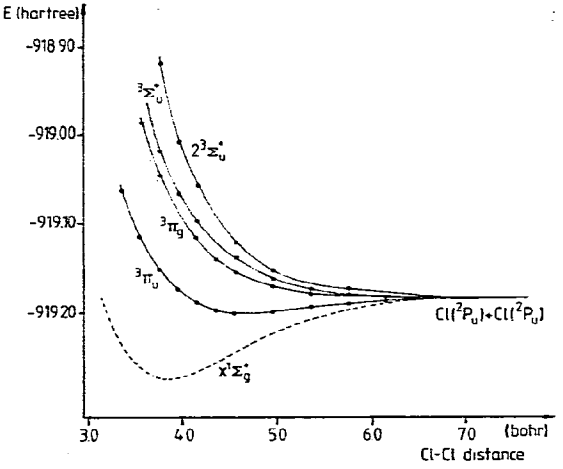

Fig. 9. Calculated potential energy curves for various triplet states of Cl_2 which dissociate into the lowest atomic limit. The corresponding ground state curve is also indicated (dashed lines). Note that not all such triplet states have been calculated.

The interaction between Rydberg and valence states in the $^3\Pi_g$ and $^3\Pi_u$ upper states runs largely parallel to the mixing in the corresponding singlet states, as seen by comparison of figs. 10 and 11 with figs. 3 and 4. The calculated dissociation limit $Cl^+(^3P_g)+Cl^-(^1S_g)$ is −918.838 hartree, i.e. 9.44 eV above the ground state products, in quite good agreement with the corresponding experimental result of (12.96 − 3.61) = 9.35 eV. The $^3\Pi_g$ is thereby the lowest of all excited Cl_2 states which dissociate to ionic products and possess definite minima at large internuclear separations. It is furthermore of special importance since it is allowed to combine with the bound lower $^3\Pi_u$ state according to the dipole selection rules. The calculated electronic energy difference between the $^3\Pi_g$ minimum ($r_e = 2.94$ Å) and the $^3\Pi_u$ at the same bond length is 4.86 eV and hence matches very well with the 258 nm (4.805 eV) laser emission.

In an attempt to obtain information regarding the $^3\Pi_g$ potential energy curve Diegelmann [4] has assumed a simple model potential based on the ionic attractive and an exponential repulsive

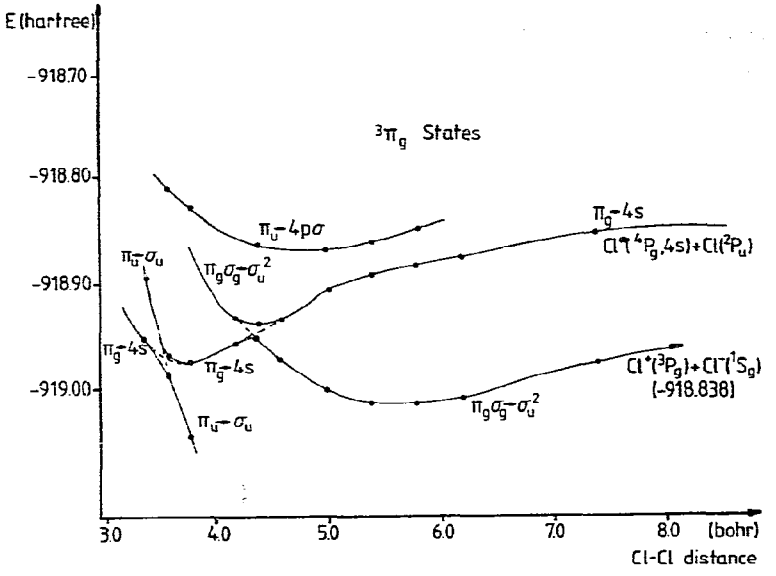

Fig. 10. Calculated potential energy curves for the lowest-lying $^3\Pi_g$ states of Cl_2 illustrating the mixing of Rydberg and valence states in this molecule.

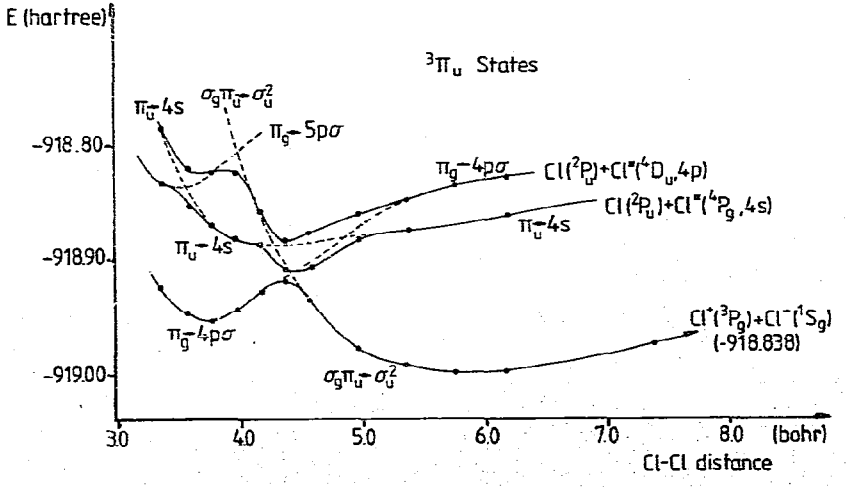

Fig. 11. Calculated potential energy curves for the lowest-lying $^3\Pi_u$ states of Cl_2 illustrating the mixing of Rydberg and valence states in this molecule.

part, thereby deriving an equilibrium distance of 2.543 Å. This finding is considerably smaller than the presently calculated value, most probably because the ionic contribution is weighted too heavily and the charge equalization which already takes place at intermediate distances is not taken properly into account. Finally, the $^3\Pi_u$ ionic state with a somewhat larger equilibrium bond length might also be of importance since it combines with almost equal intensity with the lower—albeit repulsive—$^3\Pi_g$ state as does $^3\Pi_g$–$B\,^3\Pi_u$, as will be discussed in part 2 of this work.

7. Vertical excitation energies

The combined results of all calculations are summarized in fig. 12, whereby some of the complicated structure caused by the various avoided crossings between Rydberg and valence species is omitted. The electronic energy differences relative to the ground state minimum are collected in table 11 for further quantitative use. The first allowed transition into a potential well is seen to lead to $^1\Pi_u(\pi_g \rightarrow 4p\sigma)$ and $^1\Sigma_u^+(\pi_g \rightarrow 4p\pi)$ Rydberg states at 9.16 and 9.24 eV respectively, whereby both states lie so

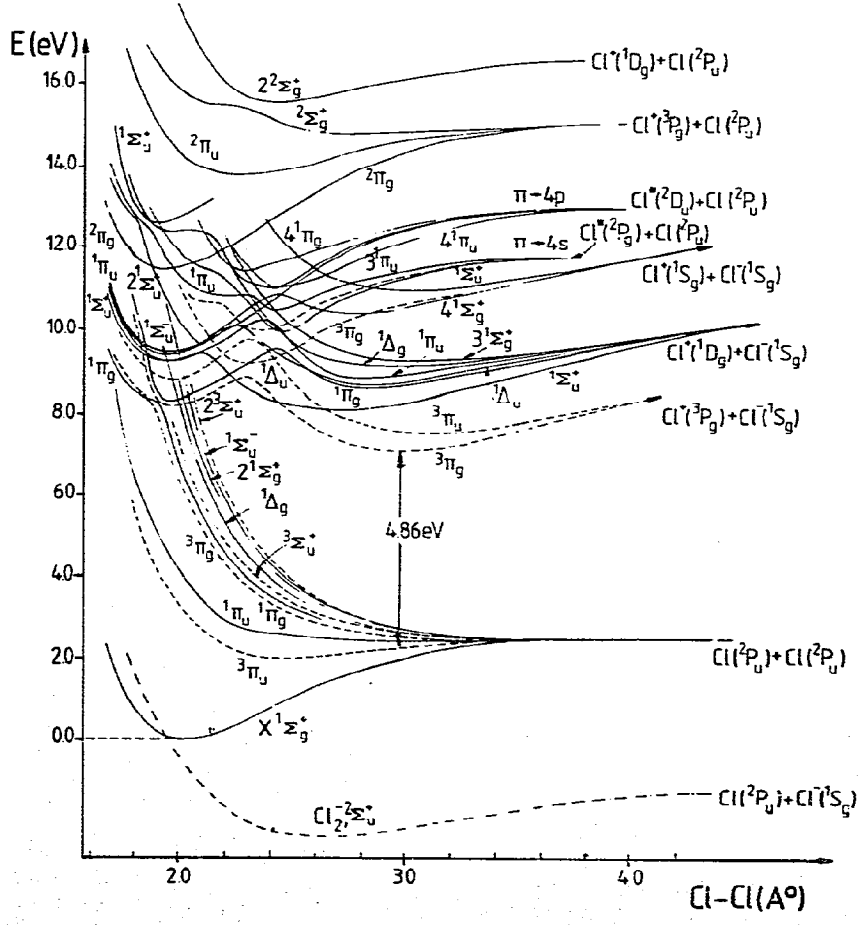

Fig. 12. Composite potential energy diagram for most of the Cl_2 states treated in the present calculations.

Table 11
Vertical electronic energies ΔE_e (in eV) from the ground state of Cl_2 to various excited states obtained at the MRD and estimated full CI level ($R = 1.988$ Å)

State	Excitation	E (MRD-CI)	E_e (full CI est.)
$X^1\Sigma_g^+$		0.00 (−919.2433)	0.00 (−919.2750)
$1^3\Pi_u$	$\pi_g \rightarrow \sigma_u$	3.24	3.31
$1^1\Pi_u$	$\pi_g \rightarrow \sigma_u$	4.04	4.05
$1^3\Pi_g$	$\pi_u \rightarrow \sigma_u$	6.23	6.29
$1^1\Pi_g$	$\pi_u \rightarrow \sigma_u$	6.86	6.83
$1^3\Sigma_u^+$	$\sigma_g \rightarrow \sigma_u$	6.80	6.87
$^1\Delta_g$	$\pi_g^2 \rightarrow \sigma_u^2$	8.25	8.12
$2^3\Pi_g$	$\pi_g \rightarrow 4s$	(8.34)	(8.21)
$2^1\Pi_g$	$\pi_g \rightarrow 4s$	(8.38) [a] 7.93	(8.22) [a] 7.81
$^1\Delta_g$	$\pi_g^2 \rightarrow \sigma_g^2$	8.25	8.12
$2^1\Sigma_g^-$	$\pi_g^2 \rightarrow \sigma_u^2$	8.35	8.29
$2^3\Pi_u$	$\pi_g \rightarrow 4p\sigma$	8.80	8.75
$2^1\Pi_u$	$\pi_g \rightarrow 4p\sigma$	9.22	9.16
$1^1\Sigma_u^+$	$\pi_g \rightarrow 4p\pi$	9.32	9.24
$1^1\Sigma_u^-$	$\pi_g \rightarrow 4p\pi$	9.58	9.43
$1^1\Delta_u$	$\pi_g \rightarrow 4p\pi$	9.62	9.47
$2^1\Sigma_u^-$	$\pi_u\pi_g \rightarrow \sigma_u^2$	9.67	9.69
$2^3\Sigma_u^+$	$\pi_u\pi_g \rightarrow \sigma_u^2$	9.75	9.74
$^1\Delta_g$	$\pi_g \rightarrow 4d\pi$	9.92	9.82
$^1\Pi_g$	$\pi_g \rightarrow 4d\sigma$	10.01	9.89
$^1\Pi_g$	$\pi_g \rightarrow 4d\delta$	10.10	10.04
$2^1\Sigma_u^-$	$\sigma_g \rightarrow \sigma_u$ / $\pi_g \rightarrow 4p\pi$	10.34	10.21
$3^3\Pi_u$	$\pi_u \rightarrow 4s$	(11.33) [a]	(11.04) [a]
$3^1\Pi_u$	$\pi_u \rightarrow 4s$	(11.51) [a] 10.95	(11.24) [a] 10.82
$^1\Pi_u$	$\pi_u \rightarrow 4d\delta$	12.74	12.64

[a] Calculations for 4s-type Rydberg states in the AO basis without d type diffuse functions; total energies of these states are generally 0.4 eV higher than in the larger basis with the more flexible s representation.

close together that the calculations are not able to definitely fix the relative ordering. Both transition energies match very well with the absorption features found recently by synchrotron radiation [28] between 1300 and 1350 Å (9.53 and 9.18 eV). Further transitions from the ground state are allowed to the $2^1\Sigma_u^+$ at 10.21 eV, which have also recently been observed [28] in the 128–122 nm region (9.68–10.16 eV). These latter excitations are fully analogous to the $2^3\Sigma_u^- - X^3\Sigma_g^-$ absorption features in oxygen, generally known as "longest", "second" and "third" peak corresponding to $2^3\Sigma_u^-(v' = 0, 1, 2)$.

In the higher-energy range states originating from depopulating the π_u MO are found in addition to $\pi_g \rightarrow 4d$ species, whereby of the latter type only a few are actually calculated. All such Rydberg transitions from $X^1\Sigma_g^+$ are forbidden by the dipole selection rules and hence presumably do not play a significant role in the Cl_2 absorption spectrum. Consistent with previous experience the splittings among the various 4d components are found to be quite small, with all such calculated species falling within 0.2 eV of one another (table 11). The only 4d transition (δ) from π_u which has been calculated is found to lie some 2.7 eV above the corresponding $\pi_g \rightarrow 4d$ species, as would be expected based on the calculated difference in the π_g and π_u ionization potentials (2.75 eV, table 6). The next allowed band system above 10.16 eV appears to be due to $\pi_u \rightarrow 4s$ transitions, whereby in the best treatment carried out the singlet species of this type possesses a vertical transition energy of 10.82 eV.

8. Summary and outlook

The present work has studied all singlet Cl_2 states which dissociate into the ground state products $Cl(^2P_u) + Cl(^2P_u)$ and the ionic species $Cl^-(^1S_g) + Cl^+(^1D_g)$. All such states which correlate with the ground state atomic products are repulsive (with the possible exception of the $^1\Pi_u$, for which the calculations show an extremely flat but yet repulsive curve). The singlet states which correlate with the ionic products show heavy interaction with the Rydberg states, giving rise to various avoided crossings and hence double-minimum potential wells. None of these states has been characterized in earlier work, either experimentally or theoretically, to the best of our knowledge.

In an analogous manner three positive ion states as well as the $^2\Sigma_u^+$ state of Cl_2^- are investigated and agreement with experiment is very good whenever comparison is possible. Only selected states of the triplet system have

been treated: the experimentally well-characterized $^3\Pi_u$ state is found to be the only bound triplet among the otherwise repulsive manifold of states dissociating into the ground state products. The two lowest-lying ionic $^3\Pi_g$ and $^3\Pi_u$ states are also observed to interact with corresponding singlet states. There is no potential data available from other theoretical or from experimental studies for any of these species, with the single exception of the $1^3\Pi_u$ state.

All electronic states have been calculated up to their dissociation limits and are quantitatively compared with the existing data for the respective isolated atomic or ionic species. The Cl_2 dissociation energy is thereby obtained as $D_e = 2.49$ eV (exptl. $D_e = 2.514$ eV), the Cl_2 electron affinity (electronic value) as 2.38 eV (exptl. 2.51 ± 0.10 eV), whereby the atomic Cl electron affinity is slightly underestimated (3.42 eV versus 3.61 eV exptl.). The $Cl^-(^1S_g) + Cl^+(^3P_g)$ dissociation limit is obtained at 9.44 eV (exptl. 9.35 eV), the $Cl^-(^1S_g) + Cl^+(^1D_g)$ at 11.02 eV (exptl. 10.79 eV)† and the $Cl^*(^2P_g, 4s) + Cl(^2P_u)$ limit is calculated to lie at 9.20 eV (above atomic ground state) compared to the measured $Cl^*(^2P_g, 4s)$ location of 9.24 eV.

The Cl_2 laser emission at 4.805 eV is found to correspond to the $2^3\Pi_g$–$1^3\Pi_u$ transition according to the present calculations, which yields a value of $\Delta E_e = 4.86$ eV (fig. 12). The absorption patterns recently found in the 130–135 nm area are suggested to arise from excitations into $^1\Pi_u$ and $^1\Sigma_u^+$ Rydberg species (9.16–9.25 eV), while the $2^1\Sigma_u^+$ state is predicted to be responsible for the higher-lying absorption in the 1.28–1.22 nm region. Emission in the singlet system most probably occurs via the ionic part of the $^1\Sigma_u^+$ and $^1\Pi_u$ states.

All evidence thus far, as well as previous experience for other systems, indicates quite strongly that the accuracy for the relative spacing of the calculated potential energy curves for neutral Cl_2 should be in the 0.1–0.2 eV range (by entirely neglecting relativistic effects), whereby somewhat larger errors are probable for the purely ionic species and high-lying states in general. In order to make a full correspondence to the various experiments under way to obtain more information on the singlet and triplet states of Cl_2, two further points must be considered in addition to the potential surfaces themselves: first, the vibrational levels should also be calculated in order to compare with the vibrational spacing of the various measured bands, and secondly, the electronic transition moment should be computed in order to predict intensities. Since most of the more interesting surfaces result from a mixing of various states, the electronic transition moment is expected to change very much over the entire range of internuclear distances, so that the Franck–Condon principle will no longer be a good approximation. Under these circumstances the actual integration over the electronic transition moment as a function of the internuclear distance folded with the respective vibrational wave-functions must be carried out explicitly in order to obtain a reliable intensity distribution. This aspect of the work will be taken up in the second part of this study.

† Note that the $^1\Sigma_u^+$ state correlating with this atomic limit is the lowest root of its symmetry and hence may be treated more accurately than the neighboring $^1\Pi_u$ and $^1\Pi_g$ states, which come as the second roots of their respective secular equations. As a result there is a possibility that the energy spread for such ionic states at intermediate R values is too large in the calculations (fig. 12).

Acknowledgement

The authors wish to thank Dr. D. Haaks (Wuppertal) for bringing to their attention the general problems associated with the Cl_2 spectrum which led to the present study. They are also indebted to him and Professor G. Zimmerer (Hamburg) for numerous valuable discussions during the course of this work. The financial support of the Deutsche Forschungsgemeinschaft in the framework of the Sonderforschungsberich 42 Program is hereby gratefully acknowledged, as are the services and computer time made available by the University of Bonn Computer Center (RHRZ).

References

[1] A.K. Hays, Opt. Commun. 28 (1979) 209.
[2] M.C. Castex, J. le Calvé, D. Haaks, B. Jordan and G. Zimmerer, Chem. Phys. Letters 70 (1980) 106.
[3] J. le Calvé, M.C. Castex, D. Haaks, B. Jordan and G. Zimmerer, Proc. European Conf. on the Dynamics of Excited States, Pisa, 1980, Nuovo Cimento, to be published.
[4] M. Diegelmann, MPI report PLF 33, August 1980, to be published.
[5] D. Haaks and G. Zimmerer, private communication.
[6] H.K. Haak and F. Stuhl, Chem. Phys. Letters 68 (1979) 399.
[7] R.J. Buenker and S.D. Peyerimhoff, Chem. Phys. Letters 36 (1975) 415.
[8] R.J. Buenker and S.D. Peyerimhoff, Chem. Phys. Letters 34 (1975) 225;
R.J. Buenker, S.D. Peyerimhoff and M. Perić, Chem. Phys. Letters 42 (1976) 383.
[9] R.S. Mulliken, Chem. Phys. Letters 46 (1977) 197.
[10] S.D. Peyerimhoff, Gaz. Chim. Italiana 108 (1978) 411.
[11] M. Yoshimine, K. Tanaka, H. Tatwaki, S. Ohara, F. Sasaki and K. Ohno, J. Chem. Phys. 64 (1976) 2254.
[12] R. Runau, S.D. Peyerimhoff and R.J. Buenker, J. Mol. Spectry. 68 (1977) 253.
[13] S.D. Peyerimhoff and R.J. Buenker, in: Computational methods in chemistry, ed. J. Bargon, IBM Research Symposia Series (Plenum Press, New York, 1980);
R.J. Buenker, S.D. Peyerimhoff and P.J. Bruna, in: Proceedings of the NATO-ASI on Theoretical Organic Chemistry, Menton, 1980;
P.J. Bruna, Gaz. Chim. Italiana 108 (1978) 395.
[14] Th. Dunning and P.J. Hay in: Modern theoretical chemistry, Vol. 3, ed. H.F. Schaefer III (Plenum Press, New York, 1977) p. 1.
[15] U. Fischbach, R.J. Buenker and S.D. Peyerimhoff, Chem. Phys. 5 (1974) 265.
[16] R.J. Buenker and S.D. Peyerimhoff, Theor. Chim. Acta 35 (1974) 33; 39 (1975) 217.
[17] R.J. Buenker, S.D. Peyerimhoff and W. Butscher, Mol. Phys. 35 (1978) 771.
[18] S.R. Langhoff and E.R. Davidson, Intern. J. Quantum Chem. 7 (1973) 999;
E.R. Davidson, in: The world of quantum chemistry, eds. R. Daudel and B. Pullmann (Reidel, Dordrecht, 1979) p. 17.
[19] S.-K. Shih, S.D. Peyerimhoff and R.J. Buenker, Chem. Phys. 17 (1976) 391.
[20] K.P. Huber and G. Herzberg, Molecular spectra and molecular structure. IV. Constants of diatomic molecules (Van Nostrand, New York, 1979).
[21] S.N. Suchard and J.E. Melzer eds., Spectroscopic data, Vol. 2 (Plenum Press, New York, 1976).
[22] C.E. Moore, Atomic energy levels I, NBS Circular 467 (1949).
[23] G. Herzberg, Molecular spectra and molecular structure. I. Spectra of diatomic molecules (Van Nostrand, New York, 1950).
[24] W. Butscher, S.-K. Shih, R.J. Buenker and S.D. Peyerimhoff, Chem. Phys. Letters 52 (1977) 457.
[25] W.A. Chupka, J. Berkowitz and D. Gutman, J. Chem. Phys. 55 (1971) 2724.
[26] L.C. Lee, G.P. Smith, G.T. Moseley, P.C. Crosby and J.A. Guest, J. Chem. Phys. 70 (1979) 3237.
[27] P.J. Bruna, S.D. Peyerimhoff and R.J. Buenker, Chem. Phys. Letters 72 (1980) 278.
[28] G. Zimmerer and D. Haaks, private communication.
[29] M.A.A. Clyne and I. McDermid, J. Chem. Soc. Faraday II 75 (1979) 1677.
[30] A.E. Douglas and A.R. Hoy, Can. J. Phys. 53 (1975) 1965.